Statistical design of chaotic waveforms with enhanced targeting capabilities

Huanan Li, Suwun Suwunnarat, and Tsampikos Kottos

Phys. Rev. B **98**, 041107 — Published 18 July 2018

DOI: 10.1103/PhysRevB.98.041107

Statistical Design of Chaotic Waveforms with Enhanced Targeting Capabilities

Huanan Li*, Suwun Suwunnarat*, Tsampikos Kottos
Physics Department, Wesleyan University, Middletown CT-06459, USA
(Dated: July 9, 2018)

We develop a statistical theory of waveform shaping of incident waves that aims to efficiently deliver energy at weakly lossy targets which are embedded inside chaotic or weakly disordered enclosures such as body cavities, buildings, vessels etc. Our approach utilizes the universal features of chaotic scattering – thus minimizing the use of information related to the exact characteristics of the chaotic enclosure. The proposed theory applies equally well to systems with and without time-reversal symmetry and will find applications in diverse areas of applied physics involving wavefront shaping for targeted energy transfer in complex environment.

PACS numbers:

Introduction –The prospect of utilizing waveform shaping of incident acoustic or electromagnetic radiation to efficiently direct energy to focal points, placed inside chaotic (or disordered) enclosures, has been recently intensely pursued [1]. The excitement for this research is twofold: On the fundamental side the interesting question is to identify schemes that will allow us to utilize multiple scattering events in complex media like disordered structures or chaotic reverberation cavities in order to overcome the diffraction limit [2–9]. A successful outcome can revolutionize many applications of wave focusing in complex media, including imaging techniques [10–13], medical therapies [14], outdoor or indoor wireless communications [15] and electromagnetic warfare [16].

In this endeavor, time reversal (TR) and wavefront shaping (WFS) are among the most promising wave-focusing schemes with impressive experimental demonstrations in a range of frequencies (see review [1]). Disregarding subtle details, it was shown that the wave focusing process is benefited from the multiple scattering events occurring during propagation inside a complex medium [1, 3, 17, 18]. These two methods are complementary in the sense that TR is a broadband approach which results in spatiotemporal focusing of incident waves while WFS is mainly a monochromatic concept which results in maxima of deposited energy at desired foci. Both methods, however, are requiring a time-reversal invariance of the propagation medium–a condition that can be violated either because of inherent losses or because of some external magnetic field. Moreover, they are not addressing the fact that in typical circumstances, where the targets are inside chaotic enclosures (or disordered enclosures of the size of the mean free path), the scattering fields demonstrate an extreme sensitivity to the exact configuration of the enclosure, its coupling to the interrogating antennas, the operating frequency etc. Thus, in many practical applications, the design of a waveform with 100% focusing efficiency (for a *specific* configuration of an adiabatically varying enclosure) is a formidable task. Instead, a more appropriate treatment would potentially rely on WFS schemes that provide maximal (not necessarily 100%) focusing efficiency and whose success is quantified using statistical tools. There are some attempts along these lines [18–21]; however a statistical approach for WFS is still lacking.

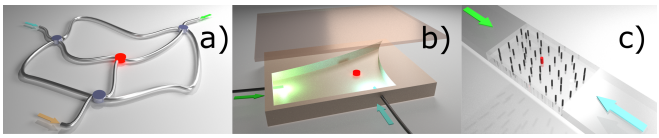

FIG. 1: (color online) A WETAC algorithm can lead to a waveform design which enhanced the probability to deliver energy at a localized lossy element (red points) embedded in (a) a complex network of coaxial cables; (b) a chaotic cavity; and (c) a multimode waveguide with random scatterers.

At the same time, there are well developed statistical methods, applicable both in the frame of electrodynamics [22, 23] and acoustics [24–26], whose central theme is the statistical description of wave interference at any position inside a complex enclosure [27, 28]. The guiding viewpoint of this school of thought is that the (adiabatic) changes of the enclosure render any attempt to describe transport characteristics for a specific "replica" of the system meaningless. Thus, the statistical description constitutes the only meaningful approach for the scattering properties of chaotic enclosures. This approach, however, does not provide any recipe for the realization of incident waveforms that will lead to foci (hot-spots) inside a chaotic/disordered enclosure.

Here we develop a *statistical* approach for the design of chaotic Waveforms with Enchanced TArgetted Capabilities (WETACs), that have high probability to deliver a large amount of their energy at localized weakly lossy targets embedded inside complex enclosures. We have used the terminology *chaotic waveform* for two reasons: (a) the designed waveforms aim to deliver maximum energy to targets inside *chaotic* or disordered enclosures of

*These authors contributed equaly. HL performed the theoretical analysis and SS the numerical analysis

the size of the mean free path (for some examples see Fig. 1), and (b) in the limit of isolated resonances these waveforms are directly related to the eigenmode components of the isolated chaotic/disordered cavity. This relation, although in a more complicated way, is also extended to the other limiting case of overlapping resonances.

Our WETAC scheme distributes the injected energy over multiple channels and utilizes the statistical features of chaotic scattering as they are quantified by the so-called Ericson parameter [28]. The design of WETACs requires a *minimal* information about the enclosure: (i) the loss-strength of the target (with some tolerance); (ii) the eigenfrequencies; and (iii) the (normalized) eigenmode amplitudes of the isolated cavity at the positions of the interrogating antennas and at the target(s). While most of this information is experimentally accessible via reflection measurements, the field amplitude at the position of the target might not be easily measured. The additional assumption that the latter is given by its ergodic limit (as it is calculated using the Random Matrix Theory formalism) is proven successful, particularly for multiple localized lossy targets. The success of the WETAC algorithms is quantified by analyzing the distribution of absorbances when the incident energy is carried over by the designed WETACs. The statistical evaluation, the Ericson parameter, and the ergodicity assumption, constitute the basic *statistical* element of the proposed scheme.

Scattering and Absorption Matrices in case of Localized Losses – The object that describes the scattering process of an incident monochromatic wave with frequency $E(k)$, is the $M \times M$ scattering matrix $S(k,\gamma)$

$$\mathcal{S}(k,\gamma) = -\hat{1} - \imath W^T \frac{1}{H_{eff}(k,\gamma) - E(k)} W, \qquad (1)$$

where M is the number of (identical) propagating channels, $\hat{1}$ is the $M \times M$ identity matrix and H_{eff}

$$H_{eff}(k,\gamma) = H(\gamma) + \Lambda(k) - \frac{\imath}{2} W W^T \qquad (2)$$

is an effective Hamiltonian that represents the cavity in the presence of radiative and Ohmic losses [29, 30]. Specifically, $H(\gamma)$ in Eq. (2) is decomposed in two terms

$$H(\{\gamma_d\}) = H_0 - \imath\Gamma_0; \quad \Gamma_0 = \sum_d \gamma_d |e_d\rangle \langle e_d|, \qquad (3)$$

where the N dimensional Hamiltonian $H_0 = H_0^\dagger$ describes the isolated system and Γ_0 indicates the existence of N_d localized lossy targets with loss-strength (Ohmic conductivity) $\gamma_d (d = 1, \cdots, N_d)$. The unit vectors $\{|e_l\rangle\}$ indicate the basis where H_0 is represented. The term $\Lambda(k)$ appearing in Eq. (2) describes the lead-coupling induced renormalization for the isolated system Hamiltonian and can be written as $\Lambda(k) = \sum_{m=1}^{M} \lambda_m(k) |e_m\rangle \langle e_m|$. The frequency-dependent real-valued constants $\lambda_m(k) = \lambda_m(-k)$ are system specific and depend on the properties of the channels and their coupling to the system. The coupling of the system with the leads is controlled by the $N \times M$ matrix W with elements $W_{lm} = \sqrt{v_g} w_m \delta_{lm}$ (w_m are dimensionless coupling strengths), where $v_g \equiv \frac{\partial E(k)}{\partial k}$.

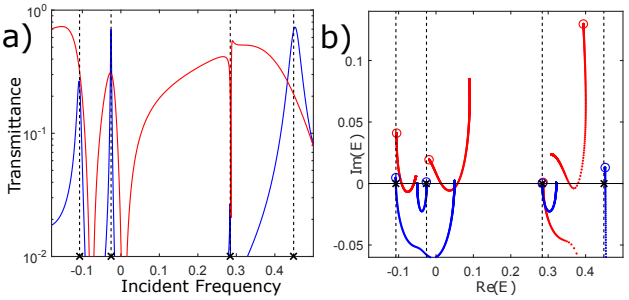

FIG. 2: (color online) (a) The transmittance versus frequency for a GOE cavity with one loss target of strength $\gamma = 0.01$. (b) The parametric evolution of complex zeros of the secular equation Eq. (6) in the complex frequency plane, as the loss-strength γ increases. The cavity is modeled by a GOE matrix H_0 with dimensionality $N = 15$, and $M = 2$ number of leads. Blue (red) lines indicate a system with a coupling constant between the leads and the cavity which is $w = 0.2$ ($w = 1$), with a corresponding Ericson parameter $\mathcal{E} \approx 0.03$ ($\mathcal{E} \approx 1.4$) indicating isolated (overlapping) resonances. The complex zeros for $\gamma = 0$ are indicated with open blue/red circles for each case respectively. Black crosses indicate the position of the eigenenergies $E_n^{(0)}$ of H_0.

For $\gamma = 0$, the scattering matrix is unitary. When $\gamma \neq 0$, it becomes sub-unitary and one can define an absorption operator $\mathcal{A} \equiv 1 - \mathcal{S}^\dagger \mathcal{S} = \mathcal{A}^\dagger$ [31]. Using Eq. (1) we get [32]

$$\mathcal{A}(k,\gamma) = 2 \sum_d \gamma_d |u_d\rangle \langle u_d|, \quad |u_d\rangle = W^T G |e_d\rangle \qquad (4)$$

where $G(k,\gamma) = \left[H_{eff}^\dagger(k,\gamma) - E(k) \right]^{-1}$.

The absorbance associated with an incident waveform $|\mathcal{I}\rangle$ is defined as

$$\alpha(k,\gamma) \equiv \frac{\langle \mathcal{I}| A(k,\gamma) |\mathcal{I}\rangle}{\langle \mathcal{I} | \mathcal{I}\rangle} \in [0,1] \qquad (5)$$

An $\alpha = 1$ indicates that the energy carried by the incident waveform is completely absorbed by the target(s). The opposite limit of $\alpha = 0$ corresponds to an incident waveform that "lost" completely the lossy target(s) and has been either transmitted or (and) reflected by the cavity. Below, we shall use α as a measure of success of a designed waveform to deliver its energy to a lossy target.

Perfect Waveforms –A perfect waveform (PW) corresponds to an incoming wave whose energy is completely absorbed by the lossy target(s). The PW $|\mathcal{I}_{PW}\rangle$ is an eigenvector $|\alpha(k_{PW},\gamma)\rangle$ of $\mathcal{A}(k_{PW},\gamma)$ with a corresponding eigenvalue $\alpha(k_{PW},\gamma) = 1$. This condition defines the

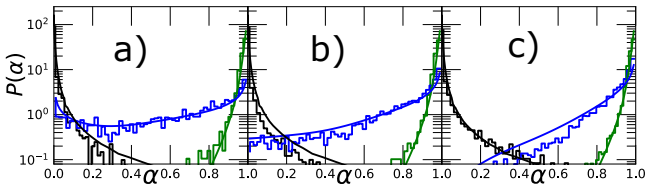

FIG. 3: (color online) Numerical (staircase lines) and theoretical (smooth lines) distribution of absorbances $\mathcal{P}(\alpha)$ for a chaotic cavity with (a) one; (b) two and; (c) four lossy targets. Green (blue) lines are associated to WETAC (ergodic WETAC) incident waveforms. Black lines are associated with an ensemble of $|\mathcal{I}_R\rangle$ incident waveforms. In all cases $M = 2, w = 0.3$ (corresponding to $\mathcal{E} \approx 0.06$). The cavities are modeled by a GOE random matrix H_0 with dimensionality $N = 15$ while $\bar{\gamma} = 0.01$ and $\eta = 0.35$.

real-valued wavevector k_{PW}. The reality of the wavevector is a physical requirement and it is associated with the fact that, in order to transport energy, the input signal has to be a propagating wave. It deserves to point out that PWs have recently attracted a lot of attention in the framework of optics where they have been identified as the time-reversed of a lasing mode [33, 34]. While these studies are restricted to integrable cavities with TR-symmetry, PWs can also emerge in chaotic systems with or without TR-symmetry [29, 30].

It is straightforward to show that, for a fixed γ, k_{PW} are the *real* zeros (if exist) of the secular equation $\det[\mathcal{S}(k,\gamma)] = 0$. Using Eq. (1) one can rewrite the secular equation in terms of the effective Hamiltonian Eq. (2) as [29, 30]

$$\zeta(k,\gamma) \equiv \det\left(H_{eff}(-k,\gamma) - E(k)\right) = 0. \qquad (6)$$

which for a fixed γ, it has multiple complex zeros k_n.

Characterization of chaotic PW based on Ericson Parameter –The scattering properties of a chaotic cavity depend crucially on the way that the system is coupled to the leads. In the case of weak coupling, the transmittance consists of resonances that demonstrate narrow linewidths Γ_n which are typically smaller than the mean level spacing Δ of the corresponding isolated cavity [28], see blue line in Fig. 2a. In the opposite limit of strong coupling, the transmittance is represented by a sum of many overlapping resonances [28], see red line in Fig. 2a.

The distinction between these two qualitative different scattering domains is typically done by the Ericson parameter $\mathcal{E} \equiv \langle\Gamma\rangle/\Delta$ where $\langle\Gamma\rangle$ is the mean resonance width. When $\mathcal{E} \ll 1$ the resonances are well isolated from one another while in the opposite case we have strongly overlapping resonances.

It turns out that the Ericson parameter controls the nature of the PW as well. In Fig.2b we show the parametric evolution of the complex zeros in the $\mathcal{R}e(E) - \mathcal{I}m(E)$-plane as the loss-strength γ increases. At the same figure we also mark with crosses the eigenvalues $\{E_n^{(0)}\}$ of the Hamiltonian H_0. Initially (i.e. for $\gamma = 0$) the zeros are in the upper part of the complex plane (see blue and red circles). As γ increases they move downwards and cross the real axis at $E_{PW} \equiv E(k_{PW})$ corresponding to a critical value of $\gamma = \gamma_{PW}$. It is exactly this pair of (E_{PW}, γ_{PW}) for which a PW can be achieved. When $\mathcal{E} \ll 1$ (blue trajectories), the E_{PW} (whenever they exist) are very close to the eigenvalues $\{E_n^{(0)}\}$ of the isolated system. In the opposite limit of $\mathcal{E} \gg 1$, the PW energies E_{PW} occur between two nearby eigenfrequencies $\{E_n^{(0)}\}$ indicating that more than one mode might affect their formation.

Design schemes for WETACs –We start our analysis with the observation that a WETAC can be determined by a subset of the normalized eigenmodes $\left|\Psi_n^{(0)}\right\rangle$ of the Hamiltonian H_0. The size $\mathcal{N}$ of this subset depends on the Ericson parameter as $\mathcal{N} = [\mathcal{E}] + 1$, where $[\cdots]$ indicates integer part. This reduced subspace is defined by a projection operator $P_{n_0}^{(\mathcal{N})} = \sum_{n=1}^{\mathcal{N}} \left|\Psi_{n_0+n}^{(0)}\right\rangle \left\langle\Psi_{n_0+n}^{(0)}\right|$ where $n_0 = 1, \cdots N - \mathcal{N}$.

Next, we project Eq. (6) in the $P_{n_0}^{(\mathcal{N})}$ subspace. The corresponding matrix elements of the reduced effective Hamiltonian $H_{eff,n_0}^{(\mathcal{N})}(-k,\gamma) = P_{n_0}^{(\mathcal{N})} H_{eff}(-k,\gamma) P_{n_0}^{(\mathcal{N})}$ are expressed in terms of the eigenvalues $\{E_n^{(0)}\}$ and eigenvectors $\{\left|\Psi_n^{(0)}\right\rangle\}$ of the isolated system which belongs to the $P_{n_0}^{(\mathcal{N})}$ subspace

$$\left[H_{eff,n_0}^{(\mathcal{N})}(-k,\gamma)\right]_{nl} = E_n^{(0)}\delta_{nl} - \imath\sum_d \gamma_d \left\langle\Psi_n^{(0)}\middle|e_d\right\rangle \left\langle e_d\middle|\Psi_l^{(0)}\right\rangle + \sum_m \left(\lambda_m(k) + \frac{\imath}{2} v_g(k) w_m^2\right) \left\langle\Psi_n^{(0)}\middle|e_m\right\rangle \left\langle e_m\middle|\Psi_l^{(0)}\right\rangle \qquad (7)$$

where the indexes d, m run over the position of the target(s) and the leads respectively. The potential WETAC pairs $(E_{WETAC}, \gamma_{WETAC})$ are associated with the real roots of the reduced secular equation $\zeta_{n_0}^{(\mathcal{N})}(E,\gamma) \equiv \det\left(H_{eff,n_0}^{(\mathcal{N})}(-k,\gamma) - E(k)\right) = 0$. Below we assume that the analysis applies for all subspaces n_0.

Out of all possible pairs $(E_{WETAC}, \gamma_{WETAC})$ which are solutions of the secular equation $\zeta^{(\mathcal{N})}(E,\gamma) = 0$ we consider only the ones that satisfy the following "proximity" constrains: (a) $E_{WETAC} \in [E_{min}^{(0)} - \delta, E_{max}^{(0)} + \delta]$ where $E_{min/max}^{(0)}$ are the borders of the frequency interval associated with the eigenmodes of the reduced subspace $P^{(\mathcal{N})}$ and $\delta \ll \Delta$; and (b) the evaluated $\gamma_{WETAC} \in \bar{\gamma}[1-\eta, 1+\eta]$ where $\bar{\gamma}$ is the loss strength (conductivity) of the target and η is a tolerance level of our knowledge of its loss-strength. The corresponding subspace $P_{\rm WETAC}^{(\mathcal{N})}$ which leads to a secular equation with solutions $(E_{WETAC}, \gamma_{WETAC})$ that satisfy the above two constrains constitute a good basis for the description of WETACs. The WETAC waveforms $|I_{\rm WETAC}\rangle$ correspond to the eigenvector $\left|\alpha_{\rm max}^{(\mathcal{N})}\right\rangle$ associated with the

maximum eigenvalue $\alpha_{\max}^{(\mathcal{N})}=1$ of the projected absorption operator $\mathcal{A}^{(\mathcal{N})}$. The latter is given by Eq. (4) with G substituted by $G^{(\mathcal{N})}\equiv P_{\rm WETAC}^{(\mathcal{N})}GP_{\rm WETAC}^{(\mathcal{N})}$.

Ergodic WETACs –In many practical situations, it is impossible to have information about the eigenmode amplitudes at the position of the target(s). We have therefore relax further the WETAC scheme by substituting in Eq. (7) for $H_{eff}^{(\mathcal{N})}$ (and consequently in $G^{(\mathcal{N})}$), the eigenmode amplitudes at the position of the target(s) with their ergodic limit i.e. $\left\langle e_d\right|\left.\Psi_l^{(0)}\right\rangle\sim 1/\sqrt{N}$. This approximation is justified for chaotic cavities where typically the modes are ergodically distributed over the enclosure. We shall refer to this algorithm as the *ergodic* WETAC.

Numerical Examples –We tested the proposed WETAC schemes for cavities with $\mathcal{E}\ll 1$ (isolated resonances) and $\mathcal{E}>1$ (overlapping resonances) as well as for cavities with and without TR-invariance. We have modeled the complex enclosures by an ensemble of $N\times N$ random matrices H_0 taken from the Gaussian Orthogonal/Unitary Ensemble (GOE/GUE) for isolated cavities with/without TR symmetry [27, 28].

When $\mathcal{E}<1$ the dimensionality of the projected subspaces is $\mathcal{N}=1$ and thus $P_n^{(\mathcal{N}=1)}=\left|\Psi_n^{(0)}\right\rangle\left\langle\Psi_n^{(0)}\right|$ for $n=1,\cdots,N$. In this case the evaluation of $H_{eff}^{(\mathcal{N}=1)}$ requires only the knowledge of the field *intensities* at the positions of the targets and of the antennas, see Eq. (7).

Following the WETAC recipe we first identify a potential pair $(E_{WETAC},\gamma_{WETAC})$. The latter is calculated from the reduced secular equation $\zeta^{(\mathcal{N})}(E,\gamma)=\left(\mathcal{R}e\left[\zeta^{(\mathcal{N})}\right],\mathcal{I}m\left[\zeta^{(\mathcal{N})}\right]\right)=(0,0)$. The pair is accepted as a WETAC solution if it satisfies the proximity constraints mentioned above. In this case the subspace $P_n^{(\mathcal{N}=1)}$ is identified as $P_{WETAC}^{(\mathcal{N}=1)}$ and is used for the evaluation of the WETAC field via $\mathcal{A}^{(\mathcal{N}=1)}$. We get

$$\left|\mathcal{I}_{WETAC}\right\rangle\propto W^T\left|\Psi^{(0)}\right\rangle \tag{8}$$

where we have used Eq. (4) together with the substitution of G with $G^{(\mathcal{N}=1)}=\left[\left\langle\Psi^{(0)}\right|G\left|\Psi^{(0)}\right\rangle\right]\left|\Psi^{(0)}\right\rangle\left\langle\Psi^{(0)}\right|$. Notice that $\left|\mathcal{I}_{WETAC}\right\rangle$ involves only the eigenmode components at the position where the leads are attached to the cavity. The latter can be measured via reflection measurements, see Ref. [28].

The efficiency of the WETAC scheme is evaluated by calculating the distribution of absorbances $\mathcal{P}(\alpha)$ for incident waveforms given by Eq. (8). In Figs. 3a,b,c we show the numerical results for $\mathcal{P}(\alpha)$ (staircase green lines) and $N_d=1,2,4$ hot-spots respectively. These distributions have been generated over a GOE ensemble of H_0 (for a fixed loss-strength $\bar{\gamma}$) by substituting Eq. (8) together with the value of E_{WETAC} satisfying the proximity constraints, in Eq. (5) for the numerical evaluation of the absorbance. In the same figure we also report the theoretical results (green lines) of $\mathcal{P}(\alpha)$ for the $\mathcal{E}<1$ WETAC scenario [32].

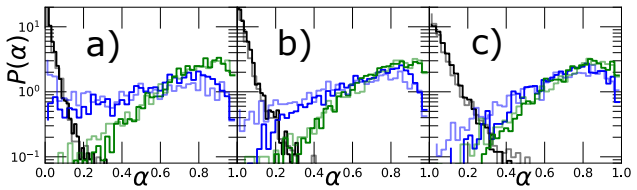

FIG. 4: (color online) Absorbance distributions $\mathcal{P}(\alpha)$ for GOE/GUE cavities (dark/light lines) with $\mathcal{E}\approx 1.4/\mathcal{E}\approx 1.7$ ($w=1$). (a) One lossy target; (b) two lossy targets; and (c) four lossy targets. The loss tolerance is $\eta=0.3$. All other parameters and color coding are the same as in Fig. 3.

In Fig. 3 we also show the numerical (staircase black lines) and the theoretical (continous black likes - see Supplement, Eq. (S12)) distribution of absorbances $\mathcal{P}(\alpha_{\max})$ when the incident waveforms $|\mathcal{I}_R\rangle=|\alpha_{max}(k)\rangle$ correspond to eigenvectors of $\mathcal{A}(k,\bar{\gamma})$ associated with the maximum eigenvalue. The wavevectors are taken from a box distribution $k\in[0,\pi]$. We find a fast decay of $\mathcal{P}(\alpha_{\max})$ indicating that the majority of these waveforms are missing the lossy target. Notice that any other random waveform will be less efficient.

In Fig. 3, we plot the theoretical result (blue solid lines) for $\mathcal{P}(\alpha)$ [32] together with the numerical data (blue staircase lines) for the ergodic WETAC scheme. In comparison with the actual WETAC, the efficiency of the *ergodic WETAC* scheme is reduced. The origin of this deviation is associated with the statistical implementation of the proximity constraint via $\gamma_{\rm WETAC}$. The ergodic WETAC scheme is, nevertheless, far superior to the random incident waves (black lines). The efficiency is improved further when more lossy targets $N_d>1$ are considered, see Fig. 3b,c. The improvement is a direct consequence of the validation of the ergodic hypothesis in the limit of many targets $1\ll N_d\ll N$.

We have also tested our WETAC algorithm for chaotic cavities with $\mathcal{E}>1$. In this case the projected space is enlarged i.e. $\mathcal{N}>1$ and the implementation of the algorithm becomes more demanding. Nevertheless, one can easily carry over the WETAC program numerically. For demonstration purposes we have considered, a system with $M=2$ channels and $\mathcal{E}=1.4$ corresponding to $\mathcal{N}=2$. The projection operator takes the form $P^{(\mathcal{N}=2)}=\left|\Psi_n^{(0)}\right\rangle\left\langle\Psi_n^{(0)}\right|+\left|\Psi_{n+1}^{(0)}\right\rangle\left\langle\Psi_{n+1}^{(0)}\right|$ for all subsequent modes $E_n^{(0)},E_{n+1}^{(0)}$ of the isolated cavity H_0. The potential WETAC pairs $(k_{WETAC},\gamma_{WETAC})$ are obdained via Eqs. (6,7). Furthermore, the implementation of the proximity conditions allow us to single out the actual WETAC pairs and the corresponding WETAC subspaces $\mathcal{P}_{WETAC}^{(2)}$.

The design of the WETAC waveforms requires the diagonalization of the reduced absorption matrix $\mathcal{A}^{(\mathcal{N}=2)}$ in the WETAC subspaces $\mathcal{P}_{WETAC}^{(2)}$. The latter are cal-

culated using Eqs. (4, 7). The eigenvector $|\alpha_{\max}\rangle$ associated with the eigenvalue $\alpha = 1$ gives us the desired WETAC $|\mathcal{I}_{\rm WETAC}\rangle = |\alpha_{\max}\rangle$. For one lossy target at position d_0 one has $|\mathcal{I}_{WETAC}\rangle \propto |u_{d_0}\rangle$ (see Eq. (4)), which in the $\mathcal{P}^{(2)}_{WETAC}$ space reads [32]

$$|\mathcal{I}_{WETAC}\rangle \propto \left(\left[H^{(\mathcal{N}=2)}_{eff}\right]_{2,2} - E_{WETAC}\right) W^T \left|\Psi^{(0)}_1\right\rangle - \left[H^{(\mathcal{N}=2)}_{eff}\right]_{2,1} W^T \left|\Psi^{(0)}_2\right\rangle . \quad (9)$$

where $H^{(\mathcal{N}=2)}_{eff}$ has been evaluated at $(k_{WETAC}, \gamma_{WETAC})$, see Eq. (7). For more lossy targets $N_d > 1$, the waveforms $|\mathcal{I}_{WETAC}\rangle$ are more complicated. Nevertheless, they can be evaluated numerically using the aforementioned WETAC algorithm. We point out that, as opposed to Eq. (8), here the calculated E_{WETAC} is affecting the WETAC waveform via the weight between the two contributing eigenmodes.

In Figs. 4a,b,c we report our numerical results for $\mathcal{P}(\alpha)$ when a WETAC incident wave is launched towards the complex cavity (green staircase) with $N_d = 1, 2, 4$ lossy targets, respectively. At the same subfigures we report also the $\mathcal{P}(\alpha)$ associated with an ergodic WETAC (blue staircase). The two approaches converge rapidly to the same distribution $\mathcal{P}(\alpha)$ as N_d increases. As a reference we also show the distribution $\mathcal{P}(\alpha)$ corresponding to random incident waveforms $|\mathcal{I}_R\rangle$ (black staircase).

WETACs for cavities with broken TR-invariance – In Fig. 4 we also report $\mathcal{P}(\alpha)$ for enclosures with broken TR-symmetry. The corresponding incident waveforms have been generated using the same WETAC scheme as above for $\mathcal{E} = 1.7$. We find that the WETAC (light green staircase) and the ergodic WETAC (light blue staircase) schemes demonstrate the same level of efficiency as in the GOE case. Light black staircase lines indicate the $\mathcal{P}(\alpha)$ generated from an ensemble of $|\mathcal{I}_R\rangle$ incident waveforms and it is shown for comparison.

Conclusions – We have proposed a statistical algorithm to design waveforms that deliver, with high probability, large portion of their energy in weakly lossy targets which are embedded inside chaotic enclosures. There are many open questions that need further investigation. For example, can we guarantee simultaneous multiple strikes? How non-universal features (like scars) can be utilized for better performance? These questions will be the theme of future research in WETAC shaping.

[1] A. Mosk, A. Lagendijk, G. Lerosey, M. Fink, *Controlling waves in space and time for imaging and focusing in complex media*, Nat. Phot. **6**, 283 (2012).

[2] P. Blomgren, G. Papanicolaou, H. Zhao, *Super-resolution in time-reversal acoustics*, J. Acoust. Soc. Am. **111**, 230 (2002).

[3] M. Fink, J. de Rosny, *Time-reversed acoustics in random media and in chaotic cavities*, Nonlinearity **15**, R1 (2002).

[4] I. M. Vellekoop, A. Lagendijk, and A. P. Mosk,*Exploiting disorder for perfect focusing*, Nat. Photon. **4**, 320 (2010).

[5] E. G. van Putten, D. Akbulut, J. Bertolotti, W. L. Vos, A. Lagendijk, and A. P. Mosk, *Scattering Lens Resolves Sub-100 nm Structures with Visible Light*, Phys. Rev. Lett. **106**, 193905 (2011).

[6] O. Katz, E. Small, Y. Bromberg, Y. Silberberg, *Focusing and compression of ultrashort pulses through scattering media*, Nat. Photonics **5**, 372 (2011).

[7] Y. Choi, T. D. Yang, C. Fang-Yen, P. Kang, K. J. Lee, R. R. Dasari, M. S. Feld, W. Choi, *Overcoming the Diffraction Limit Using Multiple Light Scattering in a Highly Disordered Medium*, Phys. Rev. Lett. **107**, 023902 (2011).

[8] P. del Hougne, F. Lemoult, M. Fink, G. Lerosey, *Spatiotemporal Wave Front Shaping in a Microwave Cavity*, Phys. Rev. Lett. **117**, 134302 (2016).

[9] C. W. Hsu, S. F. Liew, A. Goetschy, H. Cao, A. D. Stone, *Correlation-enhanced control of wave focusing in disordered media*, Nat. Physics **13**, 497 (2017).

[10] M. Fink, D. Cassereau, A. Derode, C. Prada, P. Roux, M. Tanter, J.-L. Thomas, F. Wu, *Time-reversed acoustics*, Rep. Prog. Phys. **63**, 1933 (2000)

[11] L. Borcea, G. Papanicolaou, C. Tsogka, J. Berryman, *Imaging and time reversal in random media*, Inverse Probl. **18**, 1247 (2002).

[12] G. Montaldo, P. Roux, A. Derode, C. Negreira, M. Fink, *Ultrasound shock wave generator with one-bit time reversal in a dispersive medium, application to lithotripsy*, Appl. Phys. Lett. **80**, 897 (2002).

[13] J. Dela Cruz, I. Pastirk, M. Comstock, V. Lozovoy, M. Dantus, *Use of coherent control methods through scattering biological tissue to achieve functional imaging*, Proc. Natl Acad. Sci. USA **101**, 17001 (2004).

[14] R. Horstmeyer, H. Ruan, C. Yang, *Guidestar-assisted wavefront-shaping methods for focusing light into biological tissue* , Nat. Photonics **9**, 563 (2015).

[15] A. L. Moustakas, H. U. Baranger, L. Balents, A. M. Sengupta, S. H. Simon, *Communication Through a Diffusive Medium: Coherence and Capacity*, Science **287**, 287 (2000).

[16] M. Davy, J. de Rosny, J.-C. Joly, M. Fink, *Focusing and amplification of electromagnetic waves by time reversal in an leaky reverberation chamber*, C. R. Phys. **11**, 37 (2010).

[17] P. Ambichl, A. Brandstötter, J. Böhm, M. Kühmayer, U. Kuhl, S. Rotter, *Focusing inside Disordered Media with the Generalized Wigner-Smith Operator*, Phys. Rev. Lett. **119**, 033903 (2017)

[18] S. Rotter, S. Gigan, *Light fields in complex media: Mesoscopic scattering meets wave control*, Rev. Mod. Phys. **89**, 015005 (2017).

[19] Y. D. Chong and A. D. Stone, *Hidden Black: Coherent Enhancement of Absorption in Strongly Scattering Media*, Phys. Rev. Lett. **107**, 163901 (2011).

[20] M. Davy, Z. Shi, J. Park, C. Tian, A. Z. Genack, *Universal structure of transmission eigenchannels inside opaque media*, Nat Comms **6**, 6893 (2015).

[21] B. Gerardin, J. Laurent, A. Derode, C. Prada, A. Aubry, *Full Transmission and Reflection of Waves Propagating through a Maze of Disorder*, Phys. Rev. Lett. **113**, 173901 (2014).

[22] R. Holland and R. S. John, *Statistical Electromagnetics*, Taylor and Francis, and references therein.

[23] G. Gradoni, J.-H. Yeh, B. Xiao, T. M. Antonsen, S. M. Anlage, and E. Ott, *Predicting the statistics of wave transport through chaotic cavities by the random coupling model: A review and recent progress*, Wave Motion **51**, 606 (2014).

[24] G. Tanner, N. Sondergaard, *Wave chaos in acoustics and elasticity*, Journal of Physics A: Math. Theor. **40**, R443 (2007).

[25] M. Wright, R. Weaver, *New Directions in Linear Acoustics and Vibration*, University Press Cambridge, (2010).

[26] O. Legrand, D. Sornette, *Quantum chaos and Sabine's law of reverberation in ergodic rooms*, in *Large Scale Structures in Nonlinear Physics*, Lect. Notes Phys. **392** 267 (1991).

[27] G. Akemann, J. Baik, and P. Di Francesco, *The Oxford Handbook of Random Matrix Theory* (Oxford University Press, Oxford, 2010).

[28] H. J. Stockmann, *Quantum Chaos: An Introduction*, (Cambridge University Press, Cambridge, 1999).

[29] H. Li, S. Suwunnarat, R. Fleischmann, H. Schanz, T. Kottos, *Random Matrix Theory Approach to Chaotic Coherent Perfect Absorbers*, Phys. Rev. Lett. Vol. **118**, 044101 (2017)

[30] Y. V. Fyodorov, S. Suwunarat, T. Kottos, *Distribution of zeros of the S-matrix of chaotic cavities with localized losses and coherent perfect absorption: non-perturbative results*, J. Phys. A: Math. Theor. **50**, 30LT01 (2017).

[31] Yan V. Fyodorov, *Induced vs. Spontaneous Breakdown of S-Matrix Unitarity: Probability of No Return in Quantum Chaotic and Disordered Systems*, JETP Letters **78**, 250 (2003).

[32] See Supplement.

[33] Y. D. Chong, L. Ge, H. Cao, A. D. Stone, *Coherent Perfect Absorbers: Time-Reversed Lasers*, Phys. Rev. Lett. **105**, 053901 (2010).

[34] W.Wan, Y. Chong, L. Ge, H. Noh, A. D. Stone, H. Cao, *Time-Reversed Lasing and Interferometric Control of Absorption*, Science **331**, 889-892 (2011).